ELSEVIER

Journal of Fluids and Structures 20 (2005) 505–518

JOURNAL OF FLUIDS AND STRUCTURES

www.elsevier.com/locate/jfs

Characteristics of fluid dynamic forces acting on a circular cylinder oscillated in the streamwise direction and its wake patterns

T. Nishihara[a,*], S. Kaneko[b], T. Watanabe[b]

[a]*Central Research Institute of Electric Power Industry, 1646 Abiko, Abiko-shi, Chiba 270-1194, Japan*
[b]*The University of Tokyo, 7-3-1 Hongo, Bunkyo-ku, Tokyo 113-8656, Japan*

Received 5 August 2004; accepted 19 February 2005
Available online 13 May 2005

Abstract

This paper describes the characteristics of fluid forces and wake patterns of a circular cylinder oscillating in the streamwise direction in a cross-flow, on the basis of precise measurements and flow-visualizations in forced-oscillation tests in a water tunnel at subcritical Reynolds numbers. The added mass and added damping coefficients of a circular cylinder in a streamwise oscillation were calculated. The results of the forced-oscillation tests confirmed that two reduced-velocity ranges with negative added damping exist. The two ranges agree well with the two streamwise excitation regions observed in the free-oscillation tests in several previous studies. The added mass coefficient for the streamwise vibration varies greatly, depending on the reduced velocity, and that can affect the dynamic behavior of the streamwise vibration under low mass-ratio conditions. Furthermore, the mean drag coefficient attains its maximum at the reduced velocity between the first and second excitation regions where the added damping coefficient reaches its local maximum. This suggests that the increase in the mean drag coefficient induced by the formation of alternate vortices magnifies the fluid damping effect and contributes to the damping region between the first and second excitation region.

1. Introduction

Vortex-induced vibrations (VIV) of a circular cylinder in a cross-flow, which has been one of the most challenging issues for a number of researchers, is also of practical importance for maintaining the integrity of various engineering structures subjected to flow. A number of studies conducted on VIV have been comprehensively reviewed by Sarpkaya (1979, 2004), Bearman (1984), Blevins (1990), Griffin and Hall (1995) and others.

While most of these studies concern VIV in the transverse flow direction, Wooton et al. (1972) and King et al. (1973) reported that VIV of a circular cylinder in the streamwise direction can occur under low mass-damping conditions. Naudascher (1987) reviewed in depth flow-induced streamwise vibrations of various kinds of cylindrical and axisymmetric bodies. In addition, intensive investigations into the streamwise vibration have been continued by several Japanese researchers (Okajima et al., 2001, 2002; Nakamura et al., 2001; Sakai et al., 2001). These investigations were in

*Corresponding author. Tel.: +81 4 7182 1181; fax: +81 4 7184 7142.
E-mail address: shake@criepi.denken.or.jp (T. Nishihara).

0889-9746/$ - see front matter © 2005 Elsevier Ltd. All rights reserved.
doi:10.1016/j.jfluidstructs.2005.02.003

response to the sodium leakage incident at the prototype fast breeder reactor ''Monju'' arising from damage to the thermowell caused by a flow-induced streamwise vibration (Morishita and Dozaki, 1998).

According to King et al. (1973) and Okajima et al. (2002), the streamwise vibration is excited in two flow velocity regions separated by $V_r \approx 2.5$; V_r is the reduced velocity defined by $V_r = U/(f_n d)$, where U is the incident flow velocity, f_n is the natural frequency of a cylinder, and d is the cylinder diameter. In the lower velocity region of $V_r = 1.2$–2.5 (called the ''first excitation region''), symmetric vortex shedding is usually observed, while alternate vortex shedding is observed in the higher velocity region of $V_r > 2.5$ (the ''second excitation region'').

With regard to the underlying mechanism of the first excitation region, Sarpkaya (1979) remarked that the excitation force originates from a periodic drag overshoot caused by symmetric vortex shedding, while Naudascher (1987) associated the fluctuating component of the drag coefficient with a periodic change in the near-wake width synchronized with the cylinder oscillation (called ''wake breathing''). As for the second excitation region, it is supposed that the excitation force mainly results from alternate vortex shedding with lock-in. In order to verify these explanations of the excitation mechanism, actual measurements of the unsteady drag force on a circular cylinder oscillating in the streamwise direction are needed, as well as investigations into the wake patterns around these two streamwise instability regions, particularly under low cylinder amplitude. The reason for this is that the maximum peak amplitude of the streamwise vibration is less than $0.2d$, while the transverse amplitude exceeds $1d$.

Tanida et al. (1973) measured the unsteady drag and lift forces on a circular cylinder forced to oscillate in the streamwise direction at the dimensionless cylinder amplitude $A^* = A/d$ of 0.14, where A is a peak amplitude. The results showed that the component of the fluctuating drag in phase with the cylinder oscillation velocity deviates toward positive from the quasi-steady value in the velocity range of the streamwise instability, though it always remains negative. Tanaka et al. (1999) conducted similar measurements at $A^* = 0.083$, and they showed that the added damping in the streamwise direction declines to slightly negative in the two streamwise excitation regions, though their data were not sufficient. As for the wake patterns, Ongoren and Rockwell (1988) conducted detailed flow visualizations around a circular cylinder oscillating in the streamwise direction at $A^* = 0.13$ and at a dimensionless frequency of 0.1–0.8 ($V_r = 1.25$–10). They classified modes of vortex shedding but did not discuss the relation between the wake patterns and fluid excitation forces. It should also be noted that, taking the results of Tanida et al. (1973) into account, an amplitude of $A^* = 0.13$ is probably not small enough for an investigation of the streamwise excitation mechanism.

In addition, recent studies by Khalak and Williamson (1999) and Govardhan and Williamson (2000, 2002), focusing on the phenomena involved under conditions of a small mass ratio, revealed some interesting characteristics; e.g., the dynamic response of the transverse vibration depends on the mass ratio due to variation of the added mass, even when the classical combined mass-damping parameter is the same. As for the streamwise vibration, such added mass effects have yet to be investigated.

Therefore, further investigations into the unsteady drag force and wake patterns where the cylinder amplitude is as low as possible are necessary to elucidate the excitation mechanism of the streamwise oscillation.

In this study, precise measurements of fluid forces on a circular cylinder forced to oscillate in the streamwise direction in a cross-flow, as well as detailed flow visualizations of the wake patterns, were carried out in a water tunnel at subcritical Reynolds numbers at low cylinder amplitudes. This paper describes characteristics of the fluid forces and wake patterns in cases of $A^* = 0.05$ and $V_r = 1.0$–6.0.

2. Experimental details

Our experiments were conducted in a vertical water tunnel of the gravitational draining type, which has been described in detail by Nishihara et al. (2003). Fig. 1 is a schematic of the water tunnel. It consists of an underground reservoir of 1700 m^3, an upper reservoir of 40 m^3, a vertical water tunnel section and a draining valve. The test-section is rectangular, 1000 mm × 500 mm in cross-section. Before the tunnel is operated, water is pumped up from the underground reservoir to the upper reservoir, with the draining valve closed. Once the upper reservoir has been filled with water, the valve is opened and the water flows into the test-section by gravity and drains into the underground reservoir through the valve. The descent rate of the water level in the upper reservoir was correlated to the incident flow velocity according to preliminary measurements by Laser Doppler velocimetry (DANTEC), and the incident flow velocity during the fluid force measurements was obtained from the descent rate of the water level. The turbulence intensity of the incident flow is about 1.5% of the mean flow velocity.

Fig. 2 is a schematic of the test-section and test cylinder. The test cylinder is a circular duralumin tube with a length of 490 mm, an outer diameter d of 50 mm, and an inner diameter of 38 mm. The surface of the cylinder is polished smooth. The cylinder is forced to vibrate sinusoidally and translationally, only in the streamwise direction at a constant cylinder

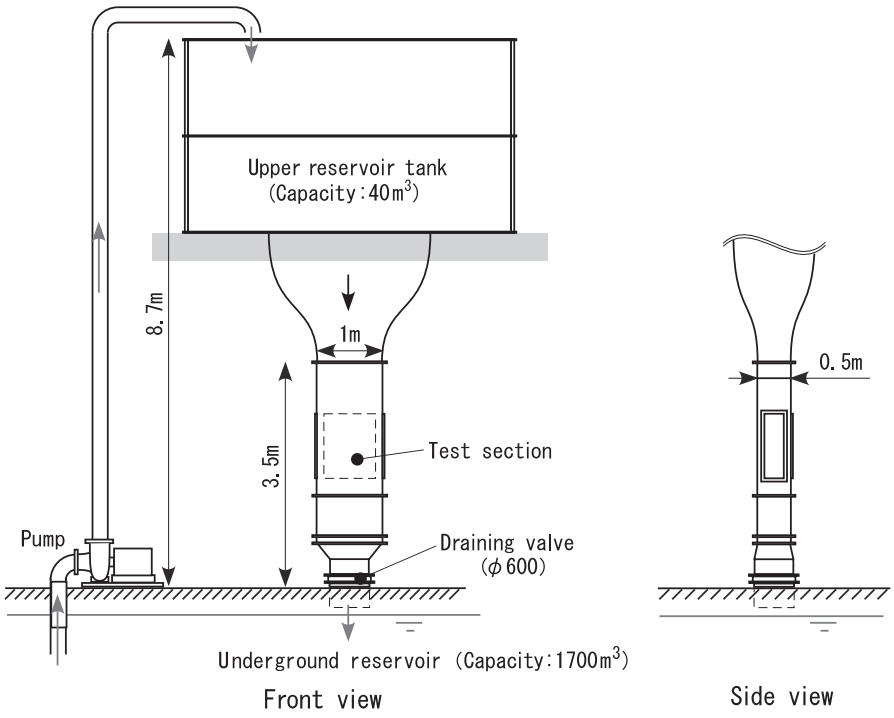

Fig. 1. Vertical water tunnel of gravitational draining type.

amplitude, by a shaker comprised of a servomotor, an eccentric cam, a crank, slide bearings and a support of phosphor-bronze. The forcing frequency f can be varied by the rotation speed of the servomotor. The clearance between the cylinder tip and sidewall is approximately 3–4 mm.

Four water-proof strain gauges were attached to the support to form a Wheatstone bridge for measuring the force on the test cylinder in each of the drag and lift directions. In preliminary calibration tests of the strain gauges, a weight was hung from the cylinder, and the outputs of strain gauges were correlated to the magnitude of the force on the cylinder per unit length. The natural frequency of the cantilevered test cylinder is 80 Hz in water. It is sufficiently higher than the forcing frequency f, so that the strain-gauge outputs during the forced-oscillation tests can be directly reduced to the dynamic force on the cylinder using the results of the static calibration tests. Moreover, the cylinder is supported so rigidly that its tip deflection amplitude during forced oscillation tests is within several percent of the forced cylinder amplitude and can thus be neglected. The displacement of the slide bearing on which the support was mounted was measured by an electrodynamic displacement sensor (Shinko Electronics A22-10C/C, SD-10T/f). The outputs of all measuring instruments were simultaneously recorded by a digital data recorder (TEAC DR-M3bMK2).

Fig. 3 is a schematic of the arrangement used in the flow visualization tests. Another cylinder and support shown on the right-hand side of Fig. 3 were used for flow visualization. The outer shape of the cylinder and support is the same as that used for the fluid force measurements. A fluorescent dye was injected through three dye outlet ports, each with a diameter of 1.5 mm, located in the middle of the cylinder in the spanwise direction as shown in Fig. 3. The injected dye was advected by the flow around the cylinder and illuminated by a Laser light sheet. The wake patterns visualized by the dye injection were taken by a high-speed CCD camera (nac, MEMRECAM Ci).

Table 1 shows the experimental conditions. The reduced velocity V_r is defined by $V_r = U/(fd)$. In the series of the experiments, the forcing frequency was varied under constant flow velocity, that is for a constant Reynolds number.

3. Preliminary tests for stationary cylinder

Measurements of fluid forces on the stationary test cylinder were preliminarily carried out prior to the forced-vibration tests. The test results are shown in Table 2, and flow patterns around the stationary cylinder are shown in

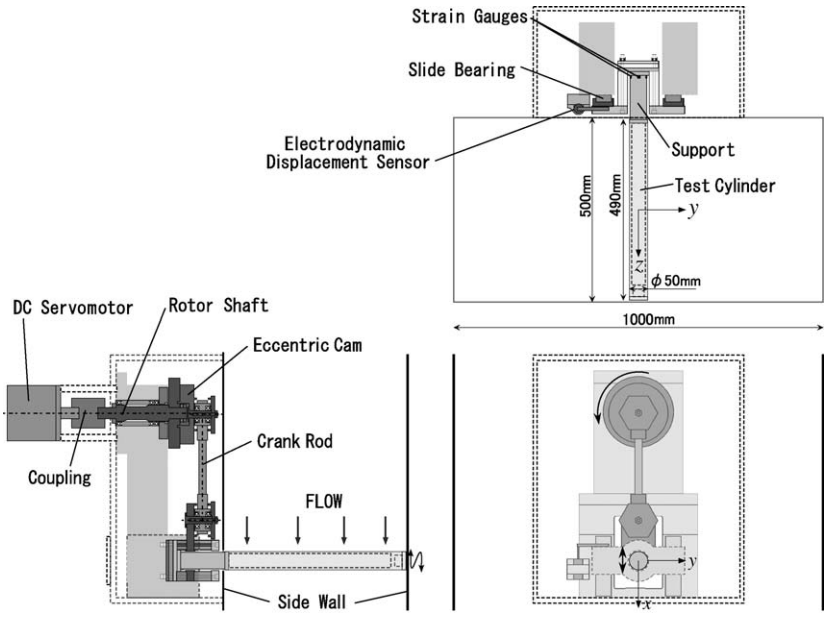

Fig. 2. Schematic of test-section and shaker.

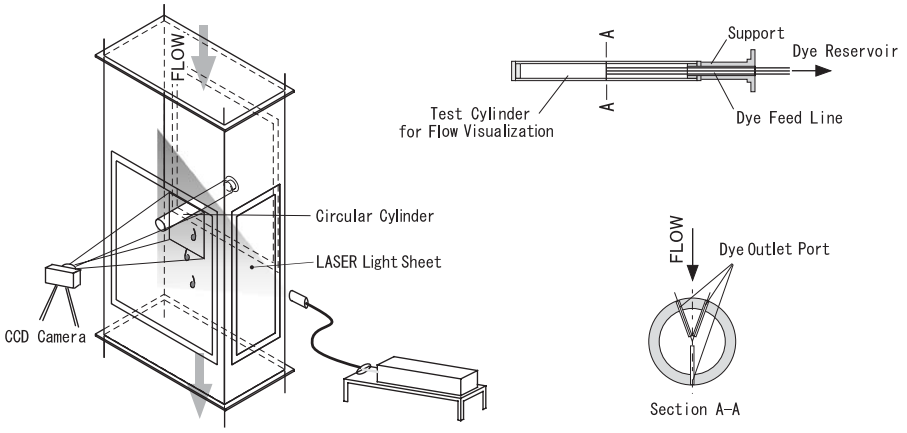

Fig. 3. Schematic of flow-visualization test.

Fig. 4 for reference in the evaluation of forced oscillation test results, described later. $\bar{C}_D$, St and $\tilde{C}_L$ are defined as follows:

$$\bar{C}_D = \bar{F}_D/(\tfrac{1}{2}\rho U^2 d), \tag{1}$$

$$\tilde{C}_L = \tilde{F}_L/(\tfrac{1}{2}\rho U^2 d), \tag{2}$$

$$\mathrm{St} = f_{L0} d/U, \tag{3}$$

where U is the incident flow velocity, and ρ is the fluid density. $\bar{F}_D$ is the mean drag per unit length, $\tilde{F}_L$ is the r.m.s. amplitude of the dynamic lift per unit length, and f_{L0} is the dominant frequency of dynamic lift on the stationary cylinder.

Table 1
Experimental conditions

Flow velocity (m/s)	0.44	0.87
Forced frequency (Hz)	2.2–9.0	2.9–14.5
Reynolds number, Re	1.7×10^4	3.4×10^4
Reduced velocity, V_r	1.0–4.0	1.2–6.0
Forced amplitude, A^*	0.05	

Table 2
Characteristics of fluid forces on the stationary test cylinder

Reynolds number, Re	1.7×10^4	3.4×10^4
Steady drag coefficient, $\bar{C}_D$	1.10	1.01
Strouhal number, St	0.184	0.182
Dynamic lift coefficient $\tilde{C}_L$	0.038	0.064

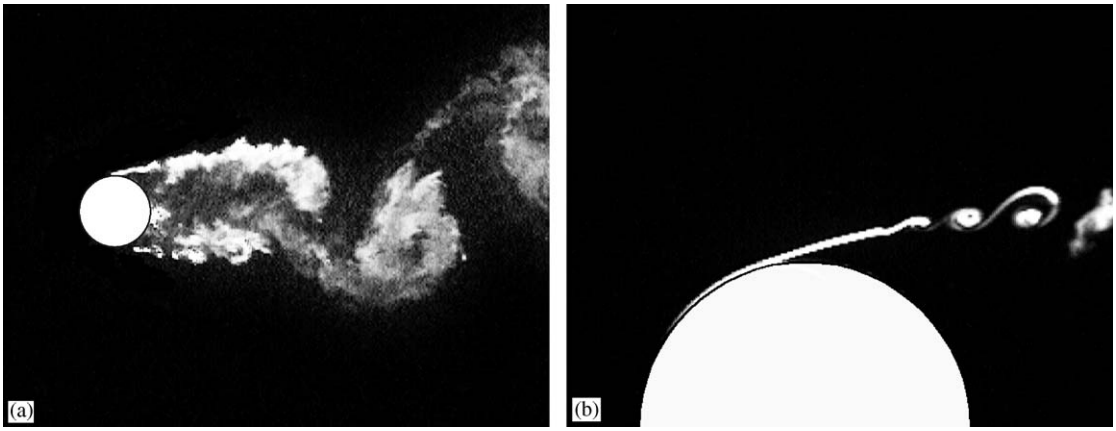

Fig. 4. Flow around stationary cylinder: (a) wake pattern; (b) close-up view of shear layer. $\mathrm{Re} = 1.7 \times 10^4$.

A typical asymmetric wake pattern can be seen in Fig. 4(a) with shear layer transition as shown in Fig. 4(b). They are reasonable flow patterns for this Reynolds number. Compared with the measurements by several researchers (Zdravkovich, 1997), the values of $\bar{C}_D$ and St are also reasonable, but the values of $\tilde{C}_L$ are rather small. The values of $\tilde{C}_L$ seem to agree with those of oblique vortex shedding, rather than those of parallel vortex shedding (Khalak and Williamson, 1996), and this is probably ascribable to end-effects.

4. Results of forced oscillation tests

In this section, the measurement results of fluid forces on the cylinder oscillated forcibly in the streamwise direction are described. Basic characteristics of the wake patterns and fluctuating lift of the test cylinder are described in Section 4.1. Characteristics of the unsteady drag force are shown in Section 4.2.

4.1. Fluctuating lift and wake patterns

Fig. 5 shows typical timetraces of the lift coefficient $C_L(t) = F_L(t)/\frac{1}{2}\rho U^2 d$, where $F_L(t)$ is lift force per unit cylinder length. Fig. 6 shows the dimensionless frequency f_L/f and the fluctuating lift coefficients $\tilde{C}_L$ versus V_r at $A^* = 0.05$,

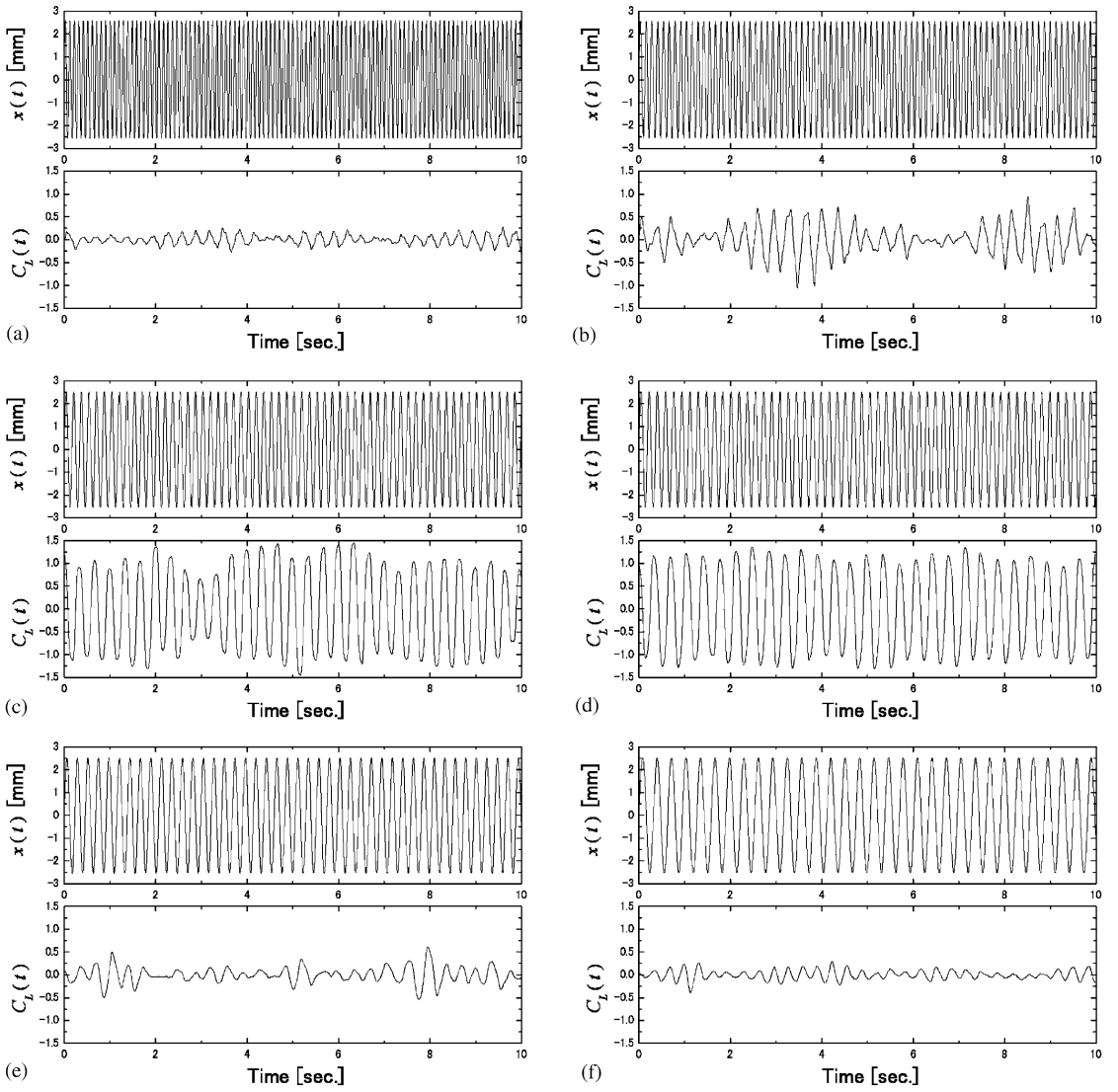

Fig. 5. Timetraces of lift coefficient $C_L(t) = F_L(t)/\frac{1}{2}\rho U^2 d$ at $\mathrm{Re} = 3.4\times10^4$: (a) $V_r = 1.7$, (b) $V_r = 2.2$, (c) $V_r = 2.9$, (d) $V_r = 3.1$, (e) $V_r = 4.0$ and (f) $V_r = 5.0$.

where f_L is the dominant frequency of the fluctuating lift, and $\tilde{C}_L$ is calculated by Eq. (2). It is seen that f_L/f is constant at 0.5 in the range of $V_r = 2.5$–3.7, that is, f_L is synchronized with $\frac{1}{2}f$. Within the lock-in range, $\tilde{C}_L$ increases significantly, compared with that in the stationary cylinder.

Typical wake patterns at $A^* = 0.05$ are shown in Fig. 7. All of these photographs were taken at the moment the cylinder was in the most downstream position. Depending on V_r, various wake patterns can be observed, and the vortex-shedding modes at $A^* = 0.05$ do not markedly differ from those obtained by Ongoren and Rockwell (1988) at $A^* = 0.13$. As described by Ongoren and Rockwell (1988), they can be basically classified into a symmetric mode of vortex shedding, an asymmetric mode, and competition of the two modes.

A symmetric mode of vortex shedding is dominant in the near-wake region at $V_r \leqslant 1.7$, and the disposition of the vortices is gradually rearranged to be asymmetric as they are advected downstream. At $V_r = 2.2$, peripatetic switches of the vortex-shedding mode between a symmetric mode and an asymmetric mode is observed. At $V_r = 2.5$ and 2.7, a well-organized asymmetric mode of vortex shedding is observed, which largely corresponds with the $\tilde{C}_L$ increases, and f_L is locked on $\frac{1}{2}f$. At $V_r = 3.1$ and 3.5, an asymmetric mode of vortex shedding is rather dominant but is less obvious than

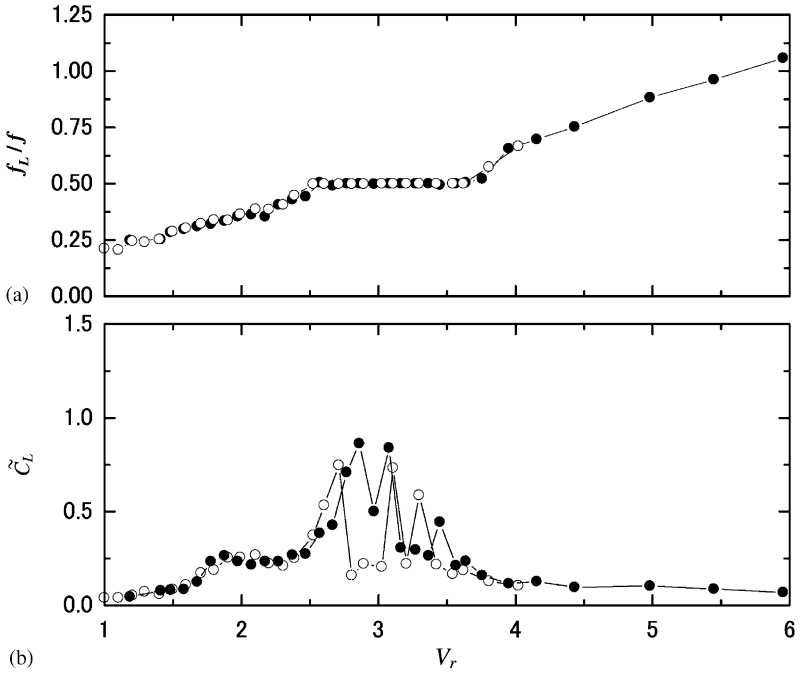

Fig. 6. Characteristics of fluctuating lift at $A^* = 0.05$. (a) Dimensionless dominant frequency f_L/f. (b) Fluctuating lift coefficient $\tilde{C}_L$. Reynolds number: $-\circ-, 1.7 \times 10^4$; $-\bullet-, 3.4 \times 10^4$.

in the case of $V_r = 2.5$ and 2.7. At $V_r \geqslant 4.0$, where it is out of the lock-in range, the wake pattern is similar to that around the stationary cylinder. Therefore, these wake patterns are in good accord with the characteristics of the measured fluctuating lift.

Thus, we have confirmed that reasonable results can be obtained by the present experimental apparatus with regard to the fluctuating lift and wake patterns.

4.2. Unsteady drag force

Here we describe the characteristics of the unsteady drag force on the cylinder oscillated in the streamwise direction, which is the main objective of this study.

The mean drag coefficient $\bar{C}_D$ and unsteady drag coefficient $\tilde{C}_D$ are calculated from the measured drag force by the following procedure. The output of strain gauges used for drag measurement during the forced oscillation tests is reduced to a force per unit length, F, according to the preliminary calibration tests. The force obtained, F, is decomposed into a time-averaged value $\bar{F}_D$ and a fluctuating component $\tilde{F}$,

$$F = \bar{F}_D + \tilde{F}. \tag{4}$$

The mean drag coefficient $\bar{C}_D$ is defined by Eq. (1).

As for the fluctuating component $\tilde{F}$, a cross-spectral analysis between $\tilde{F}$ and the oscillating displacement x of the cylinder measured by the electrodynamic displacement sensor is conducted to calculate the Fourier-averaged in-phase-with-x component, F_R, and the out-of-phase component, F_I. That is, when the cylinder is oscillating sinusoidally with an amplitude A and an angular frequency $\omega = 2\pi f$,

$$x = A\mathrm{e}^{\mathrm{i}\omega t}, \tag{5}$$

$$\tilde{F}_e = (F_R + \mathrm{i}F_I)\mathrm{e}^{\mathrm{i}\omega t}, \tag{6}$$

where $\tilde{F}_e$ is the fluctuating force synchronized with x. Since F_R includes an inertia force F_{R0} originating from the cylinder mass, F_{R0} is deducted from F_R to calculate the in-phase component, F_M, of the unsteady fluid drag on

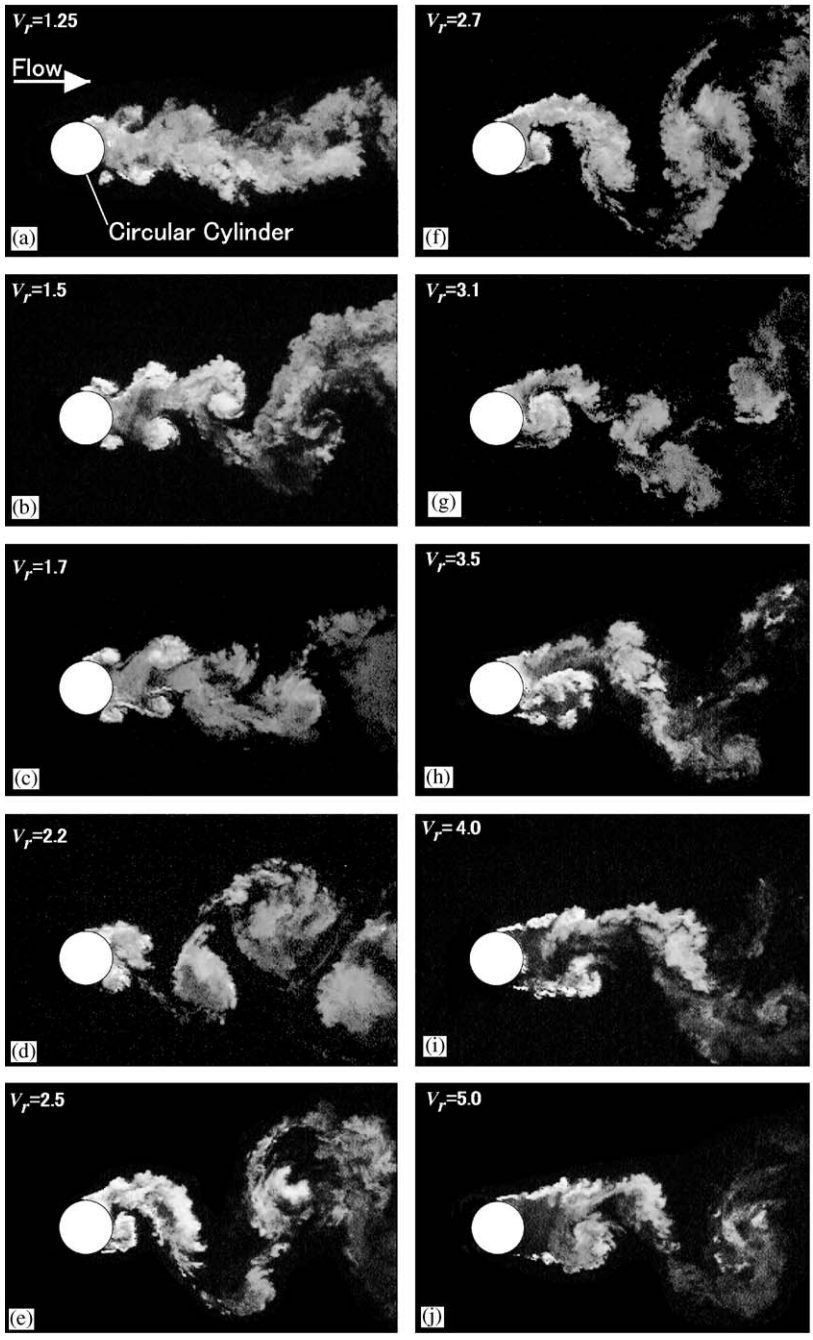

Fig. 7. Typical wake patterns at $A^* = 0.05$. Re$= 1.7 \times 10^4$.

the cylinder as follows:

$$F_M = F_R - F_{R0}. \tag{7}$$

F_{R0} was estimated by the preliminary forced-oscillation tests in the air.

The unsteady fluid drag $\tilde{F}_D$ is then expressed as

$$\tilde{F}_D = (F_M + \mathrm{i}F_I)\mathrm{e}^{\mathrm{i}\omega t}. \tag{8}$$

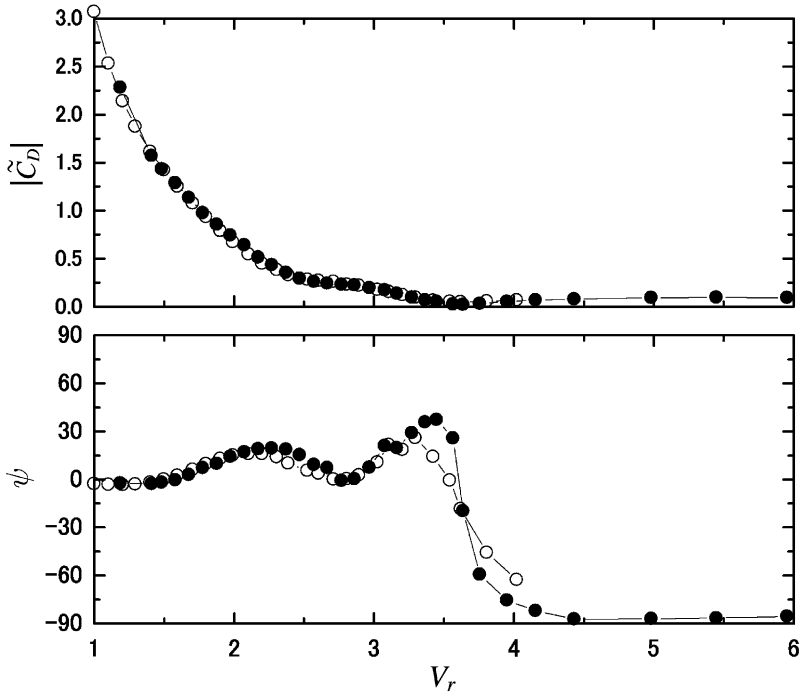

Fig. 8. Unsteady drag coefficient at $A^* = 0.05$. Reynolds number: $-\circ-$, 1.7×10^4; $-\bullet-$, 3.4×10^4.

The unsteady drag coefficient $\tilde{C}_D$ is defined as a complex number by the following equation:

$$\tilde{C}_D = (F_M + \mathrm{i}F_I)/(\tfrac{1}{2}\rho U^2 d). \tag{9}$$

The results of $\tilde{C}_D$ at $A^* = 0.05$ are shown in Fig. 8, where ψ is the phase of $\tilde{C}_D$. The amplitude of $\tilde{C}_D$ decreases as V_r increases, because $\tilde{C}_D$ includes the inertia force component due to added mass and $\tilde{C}_D$ originates mainly from the inertia force in the low V_r range. The phase ψ of $\tilde{C}_D$ is slightly negative at $V_r < 1.5$, that is, the unsteady drag acts on the cylinder as a positive damping force. At $V_r = 1.5$, ψ passes zero to become positive, which indicates that the unsteady drag force on the oscillating cylinder changes from being a damping force to an excitation force. As V_r increases, ψ rises to approximately 20° around $V_r = 2.2$ and begins to decline. After ψ falls to almost zero at $V_r = 2.7$, ψ begins to increase again, and it reaches its maximum around $V_r = 3.3$–3.5. With further increases of V_r, ψ rapidly drops to be almost −90°. The results at $\mathrm{Re} = 1.7 \times 10^4$ and 3.4×10^4 do not markedly differ from each other.

Hence, it is clearly shown that two reduced-velocity ranges exist where ψ is positive. The two ranges agree with the two streamwise excitation regions observed in the free-oscillation tests in several previous studies (King et al., 1973; Okajima et al., 2002).

5. Discussion

5.1. Added mass and added damping coefficients

As has been described, the present measurement results confirmed that two excitation regions exist in the unsteady drag force. With the expression of $\tilde{C}_D$, however, it is not easy to understand how these properties of the unsteady drag force correspond with the dynamic response of the streamwise free oscillation described in previous studies, and how they quantitatively affect the freely oscillating cylinder. Thus, here we introduce the added mass and added damping coefficients.

The equation of motion of an elastically supported rigid cylinder oscillating freely in an infinite and uniform cross-flow is expressed by the following equation:

$$m_s\ddot{x} + c_s\dot{x} + k_s x = \tilde{F}_D, \tag{10}$$

where m_s, c_s and k_s are the structural mass per unit length, structural damping, and spring constant, respectively. In general, the unsteady fluid force $\tilde{F}_D$ is expressed as

$$\tilde{F}_D = -m_a\ddot{x} - c_a\dot{x} - k_a x. \tag{11}$$

When the cylinder continues to vibrate at a constant amplitude A and an angular frequency ω as $x = Ae^{i\omega t}$, $-k_a x$ can be expressed as $k_a\ddot{x}/\omega^2$. Therefore, Eq. (11) can also be expressed as

$$\tilde{F}_D = -m'_a\ddot{x} - c_a\dot{x}. \tag{12}$$

Either Eq. (11) or Eq. (12) can be used. For this problem, however, it is not suitable to introduce the added stiffness term $-k_a x$, since the displacement of the rigid cylinder does not vary the geometry of the flow boundary or flow path, unlike in the cases of a tube bundle and a body near a wall. It is therefore appropriate to use Eq. (12) in this study. Eq. (10) can then be arranged as

$$\text{Real part:} \quad (m_s + m'_a)\omega^2 = k_s, \tag{13}$$

$$\text{Imaginary part:} \quad (c_s + c_a)\omega = 0. \tag{14}$$

Comparing Eq. (8) with Eq. (12), the following equations are obtained:

$$m'_a = F_M/\{\omega^2 A\}, \tag{15}$$

$$c_a = -F_I/\{\omega A\}. \tag{16}$$

The in-phase component F_M is thus reduced to the added mass; m'_a is sometimes called the effective added mass (Govardhan and Williamson, 2000, 2002).

The added mass coefficient C_M is then defined as follows:

$$C_M = m'_a/m_{a0}, \tag{17}$$

where m_{a0} is the displaced fluid mass $\pi\rho d^2/4$.

As for c_a, taking Eq. (13) into account, Eq. (14) is converted to the following equation:

$$4\pi\zeta_s\mu\beta(\mu) + C_a = 0, \tag{18}$$

where μ, ζ_s, β and C_a are given by

$$\mu = \frac{m_s + m_{a0}}{\rho d^2}, \tag{19}$$

$$\zeta_s = \frac{c_s}{2\sqrt{m_s k_s}}, \tag{20}$$

$$\beta(\mu) = \sqrt{\left(1 - \frac{\pi}{4\mu}\right)\left\{1 + \frac{\pi(C_M - 1)}{4\mu}\right\}}, \tag{21}$$

$$C_a = \frac{c_a}{\rho d^2 f}. \tag{22}$$

In the above, $4\pi\zeta_s\mu$ is the classical reduced damping (King et al., 1973; Blevins, 1990). C_a is the dimensionless added damping coefficient, which depends on Re, A^*, and V_r defined using the actual oscillation frequency f; β is a function of the mass ratio μ and expresses the effect of frequency variations due to added mass. It should be kept in mind that the classical reduced damping $4\pi\zeta_s\mu$ is not exactly equal to $-C_a$ in Eq. (18). Only when the mass ratio μ is high enough does β become almost 1, and $4\pi\zeta_s\mu$ become equal to $-C_a$. Additionally, c_s is treated as a constant in the formulation above, while the formulation also depends on structural damping. How to determine the damping ratio was thoroughly discussed by Sarpkaya (1979) and Nakamura et al. (2001).

Fig. 9 shows the calculated C_M and C_a along with the mean drag coefficient $\bar{C}_D$ on the basis of the present measurement.

Though C_M is almost 1 at $V_r \leqslant 2$, it decreases gradually as V_r increases, becoming almost 0 at $V_r \geqslant 3.7$. As for the transverse vibration, Sarpkaya (1979) indicated that C_M in a steady flow is no longer the same as in a still fluid. Govardhan and Williamson (2002) confirmed that the variations in C_M play an important role in the dynamic response of VIV in the transverse direction under low mass-ratio conditions. The present results clearly show that C_M for the

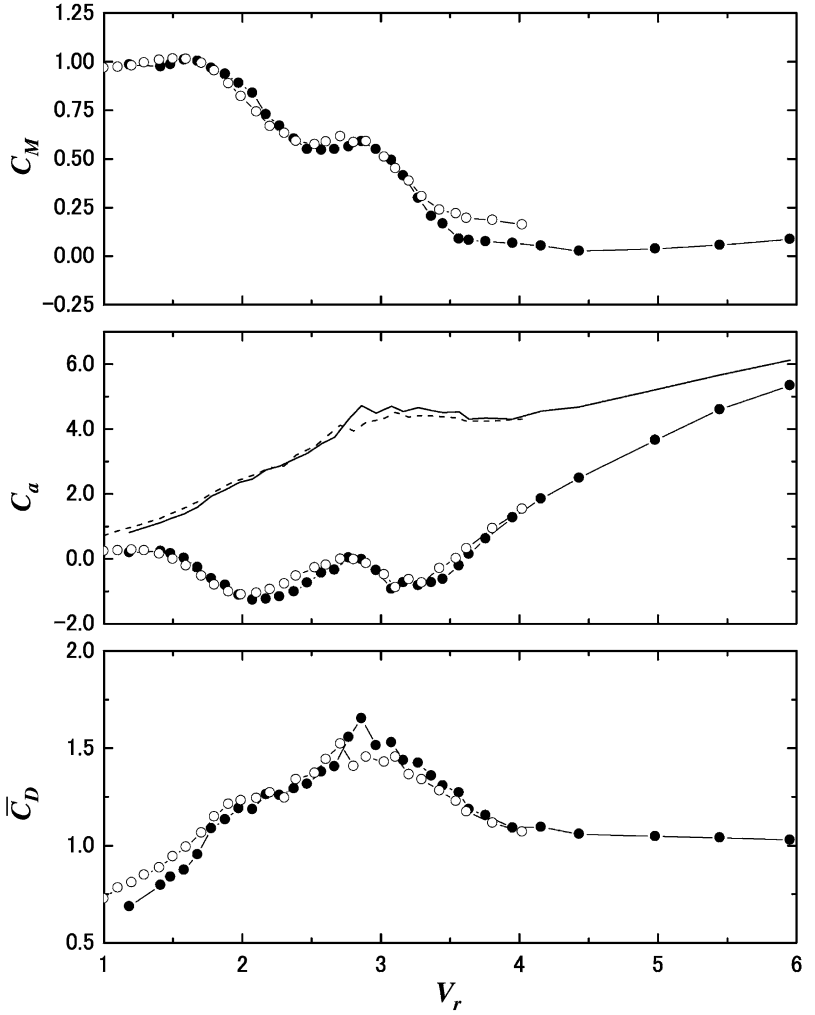

Fig. 9. Added mass and added damping coefficients along with mean drag coefficient. Reynolds number: $-\circ-, 1.7\times10^4$; $-\bullet-, 3.4\times10^4$. Broken line: quasi-steady value at Re$=1.7\times10^4$. Solid line: quasi-steady value at Re$=3.4\times10^4$.

streamwise vibration also varies greatly depending on V_r, and that may affect the dynamic behavior of the streamwise vibration in a similar way as for transverse vibration. For example, Aguirre (1977) observed that the actual frequency of the streamwise vibration tends to be higher than the natural frequency in still fluid. Such a phenomenon can reasonably be explained by the variation of C_M.

Two V_r ranges with negative C_a exist, which correspond with the two excitation regions for streamwise free-vibrations previously reported. With regard to the first excitation region, the maximum absolute value of C_a is approximately 1.0. This agrees well quantitatively with the results of free-oscillation tests by Okajima et al. (2002) that the maximum of the r.m.s dimensionless amplitude of cylinder displacement becomes larger than 3.5% when $4\pi\zeta_s\mu$ is less than approximately 1.0. As for the second excitation region, the maximum absolute value of C_a is approximately 0.9. According to the free-vibration tests by Okajima et al. (2001) and Nakamura et al. (2001), the response amplitude in the second excitation region depends on the support conditions, the aspect ratio and the end effect. The maximum r.m.s. amplitude in the second excitation region is larger than that in the first excitation region and remains at 6% when $4\pi\zeta_s\mu$ is less than approximately 1.0 for a circular cylinder supported elastically at both ends. For a cantilevered circular cylinder, the maximum r.m.s. amplitude in the second excitation region is lower than that in the first excitation region. Considering the aforementioned results by Okajima et al. (2001) and Nakamura et al. (2001), the maximum absolute value of C_a in the second excitation region obtained by the present forced-oscillation tests is also reasonable.

The broken line in the graph shows the fluid damping effect $\tilde{C}_D V_r$ based on quasi-steady theory. The graph clearly shows that C_a becomes close to the quasi-steady value where V_r is higher than 4.

5.2. Comparison between added damping coefficient and wake patterns

As described in Section 5.1, we have confirmed that the C_a obtained by the present experiments is quantitatively reasonable. Next, the relation between the wake patterns and the unsteady drag force is discussed.

Fig. 10 shows the transitions of wake patterns in the near wake during one cycle of cylinder oscillation.

Fig. 10(a) shows the transition of the wake patterns during one cycle of cylinder oscillation at $V_r = 1.7$. Such wake motions are called the "wake breathing", and a pair of symmetric vortices is shed as the cylinder moves upstream. Naudascher (1987) explained that the excitation force in the streamwise direction originates from a periodic change in the near-wake width synchronized with the cylinder oscillation, while Sarpkaya (1979) remarked that the excitation force originates from a periodic drag overshoot caused by symmetric vortex shedding. Though there is room for argument on which explanation is more reasonable, the present results of the forced-vibration tests have confirmed that such wake motions generate an excitation force at any rate.

Fig. 10(b) shows the transition of the wake patterns during an oscillation cycle at $V_r = 2.7$. As shown in Fig. 9, C_a reaches its local maximum at $V_r \approx 2.7$. The narrow range between the first and second excitation regions corresponds

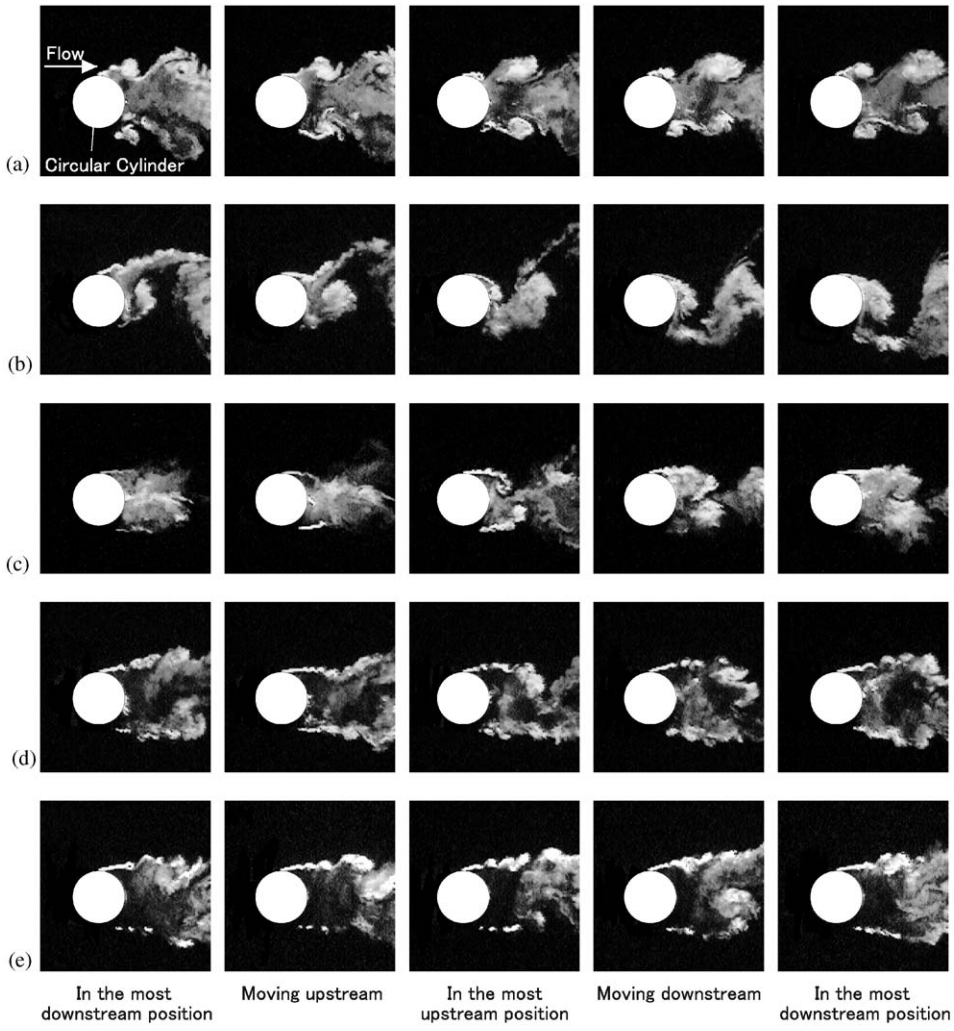

Fig. 10. Transitions of wake patterns at Re$= 1.7 \times 10^4$: (a) $V_r = 1.7$, (b) $V_r = 2.7$, (c) $V_r = 3.1$, (d) $V_r = 4.0$ and (e) $V_r = 5.0$.

to the drop in the response amplitude of the streamwise vibration in the free-oscillation tests, as reported by King et al. (1973) and Okajima et al. (2002). Naudascher (1987) reported that the sudden drop in the response amplitude of the streamwise vibration is due to incompatibility of the two vortex-shedding modes. As shown in Fig. 10(b), however, alternate vortex shedding is observed most clearly at $V_r = 2.7$. One separated shear layer is drawn toward the rear of the cylinder, and begins to roll up and form a vortex as the cylinder moves upstream. The vortex formed remains in the rear of the cylinder as the cylinder moves downstream and is advected downstream as the cylinder moves upstream. These wake motions seem to generate a streamwise excitation force, because they increase the drag force as the cylinder moves downstream and vice versa. On the contrary, the present results show that the excitation force diminishes (where C_a reaches its local maximum) at $V_r = 2.7$, i.e., the excitation force diminishes at the classical resonance condition of $f \approx 2f_{L0}$.

Fig. 10(c) shows the transition of the wake patterns during an oscillation cycle at $V_r = 3.1$, where C_a has its local minimum. In the second excitation region, alternate vortex shedding is usually observed in free-oscillation tests. In the present forced-oscillation tests, asymmetric vortex shedding is rather dominant, but is less obvious at $V_r = 3.1$ than in the case of $V_r = 2.7$. It may be proper to describe the transition of wake patterns as a combination of the wake breathing and alternate vortex shedding.

Figs. 10(d) and (e) show the transitions of the wake patterns during an oscillation cycle at $V_r = 4.0$ and 5.0, respectively. Though the wake width decreases slightly as the cylinder moves upstream, the motion of the separated shear layer is limited in the near wake, i.e. there is little change in the instantaneous flow patter. In such cases, the characteristics of the drag force can be considered as in quasi-steady theory. In fact, C_a obtained by the present measurements becomes close to the quasi-steady value at $V_r \geqslant 4.0$.

Therefore, the results of the present experiments in the first excitation region are consistent with the results of previous free-vibration tests and the description of the phenomenon in previous reports by other researchers. The wake patterns for $V_r \geqslant 4$ are also consistent with the results of the fluid force measurements. However, flow patterns in the second excitation region and the narrow range between the first and second excitation regions do not seem to be consistent with the characteristics of C_a at first glance. The reason for this is probably related with the mean drag coefficient $\bar{C}_D$. It is noted that $\bar{C}_D$ attains its maximum where C_a reaches its local maximum, as shown in Fig. 9. Naudascher and Rockwell (1994) remarked that whether the unsteady drag force acts on a cylinder as an excitation force or as a damping force depends on the relative magnitudes of two opposite effects. The first is the excitation force induced by the motion of the separated shear layer and vortices synchronized with the cylinder motion. The second is fluid damping originating from the relative velocity change between the cylinder and fluid. The correspondence between C_a and $\bar{C}_D$ at $V_r \approx 2.7$ in the present experiments implies that the increase in $\bar{C}_D$ magnifies the second effect in the narrow range between the first and second excitation regions. That is, the second effect is magnified by the increase in $\bar{C}_D$ and overcomes the first effect in this narrow V_r range, though the well-organized alternate vortex shedding also generates the first effect.

6. Conclusion

Precise measurements of fluid forces on a circular cylinder forced to oscillate in the streamwise direction in a cross-flow as well as detailed flow visualization of the wake patterns were carried out in a water tunnel at subcritical Reynolds numbers at low cylinder amplitude. The added mass and damping coefficients were estimated based on the measurement results.

The results of the forced-oscillation tests confirmed that two reduced-velocity ranges with negative added damping exist, which agrees well with the two streamwise excitation regions observed in the free-oscillation tests in several previous studies. The flow visualization tests confirmed that wake breathing and typical symmetric vortex shedding are observed in the first excitation region, whereas the combined flow patterns of wake breathing and asymmetric vortex shedding appear in the second excitation region. The maximum absolute values of added damping coefficient in the first and second excitation regions are also quantitatively reasonable, compared to the free-vibration test results by other researchers.

A well-organized alternate vortex shedding is observed most clearly when the forcing frequency f is approximately twice the natural vortex-shedding frequency f_{L0}. Though such vortex motions seem to generate an excitation force, the added damping coefficient reaches its local maximum at $f \approx 2f_{L0}$. The reason for this is probably related to the mean drag coefficient. The mean drag coefficient also reaches its maximum at $f \approx 2f_{L0}$, which implies that the increase in the mean drag coefficient magnifies the fluid damping effect originating from the relative velocity change between the cylinder and the fluid.

The added damping coefficient becomes close to the quasi-steady value when the reduced velocity is higher than 4.0. This is consistent with the wake patterns showing that the motion of the separated shear layers in the near wake is limited.

Furthermore, the added mass coefficient varies greatly, depending on the reduced velocity, and gradually decreases as the reduced velocity increases, becoming almost zero where the reduced velocity is higher than 3.7. The variation of the added mass coefficient can affect the dynamic response of the streamwise vibration especially under low mass-ratio conditions.

References

Aguirre, J.E., 1977. Flow-induced, in-line vibrations of a circular cylinder. Doctoral Dissertation, Imperial College of Science and Technology, London, UK.

Bearman, P.W., 1984. Vortex shedding from oscillating bluff bodies. Annual Review of Fluid Mechanics 16, 195–222.

Blevins, R.D., 1990. Flow Induced Vibrations. Van Nostrand Reinhold, New York.

Govardhan, R., Williamson, C.H.K., 2000. Modes of vortex formation and frequency response of a freely vibrating cylinder. Journal of Fluid Mechanics 420, 85–130.

Govardhan, R., Williamson, C.H.K., 2002. Resonance forever: existence of a critical mass and an infinite regime of resonance in vortex-induced vibration. Journal of Fluid Mechanics 474, 147–166.

Griffin, O.M., Hall, M.S., 1995. Vortex-shedding lock-on in a circular cylinder wake. In: P.W. Bearman (Ed.), Flow-Induced Vibration. Balkema, Rotterdam, pp. 3–14.

Khalak, A., Williamson, C.H.K., 1996. Dynamics of a hydroelastic cylinder with very low mass and damping. Journal of Fluids and Structures 10, 455–472.

Khalak, A., Williamson, C.H.K., 1999. Motions, forces and mode transitions in vortex-induced vibrations at low mass-damping. Journal of Fluids and Structures 13, 813–851.

King, R., Prosser, M.J., Johns, D.J., 1973. On vortex excitation of model piles in water. Journal of Sound and Vibration 29, 169–188.

Morishita, M., Dozaki, K., 1998. History of flow-induced vibration incident occurred in Monju. Flow-Induced Vibration and Transient Thermal-Hydraulics, PVP-vol. 363. ASME, New York, pp. 103–108

Nakamura, A., Okajima, A., Kosugi, T., 2001. Experiments on flow-induced in-line oscillation of a circular cylinder in a water tunnel, second report: influence of the aspect ratio of a cantilevered circular cylinder. JSME International Journal Series B 44-4, 705–711.

Naudascher, E., 1987. Flow-induced streamwise vibrations of structures. Journal of Fluids and Structures 1, 265–298.

Naudascher, E., Rockwell, D., 1994. Flow-Induced Vibrations, An Engineering Guide. Balkema, Rotterdam, pp. 56–59.

Nishihara, T., Inada, F., Yasuo, A., Morita, R., Sakashita, A., Mizutani, J., 2003. Turbulence-induced fluid dynamic forces acting on cross-shaped tube bundle in cross-flow. Journal of Fluids and Structures 18, 635–650.

Okajima, A., Kosugi, T., Nakamura, A., 2001. Experiments on flow-induced in-line oscillation of a circular cylinder in a water tunnel, first report: the difference of the response characteristics when a cylinder is elastically supported at both ends and cantilevered. JSME International Journal Series B 44-4, 695–704.

Okajima, A., Kosugi, T., Nakamura, A., 2002. Flow-induced in-line oscillation of a circular cylinder in a water tunnel. ASME Journal of Pressure Vessel Technology 124, 89–96.

Ongoren, A., Rockwell, D., 1988. Flow structure from an oscillating cylinder Part 2: mode competition in the near wake. Journal of Fluid Mechanics 191, 225–245.

Sakai, T., Iwata, K., Morishita, M., Kitamura, S., 2001. Vortex-induced vibration of a cantilevered circular cylinder in super-critical Reynolds number flow and its suppression by structure damping. JSME International Journal Series B 44-4, 712–720.

Sarpkaya, T., 1979. Vortex-induced oscillations. ASME Journal of Applied Mechanics 46, 241–258.

Sarpkaya, T., 2004. A critical review of the intrinsic nature of vortex-induced vibrations. Journal of Fluids and Structures 19, 389–447.

Tanaka, H., Tanaka, K., Shimizu, F., 1999. Vibration characteristics of a cylinder and its fluid dynamic force in a low flow velocity range. Transactions of the JSME Series B 65-640, 3933–3940 (in Japanese).

Tanida, Y., Okajima, A., Watanabe, Y., 1973. Stability of a circular cylinder oscillating in uniform flow or in a wake. Journal of Fluid Mechanics 61, 769–784.

Wooton, L.R., Warner, M.H., Cooper, D.H., 1972. Some aspects of the oscillations of full-scale piles. In: Naudasher, E. (Ed.), Flow-Induced Structural Vibrations. Springer, Berlin, pp. 587–601.

Zdravkovich, M.M., 1997. Flow Around Circular Cylinders, vol.1: Fundamentals. Oxford University Press, Oxford.